IEEE Transactions on Control Systems Technology 22(6), 2912-2917, 2014

Integral LOS Path Following for Curved Paths Based on a Monotone Cubic Hermite Spline Parametrization

Anastasios M. Lekkas and Thor I. Fossen

Abstract— **This paper addresses two interrelated problems concerning the planar three degree-of-freedom motion of a vehicle, namely, the path planning problem and the guidance problem. The monotone cubic Hermite spline interpolation (CHSI) technique by Fritsch and Carlson is employed to design paths that provide the user with better shape control and avoid wiggles and zigzags between the two successive waypoints. The conventional line-of-sight (LOS) guidance law is modified by proposing a time-varying equation for the lookahead distance, which is a function of the cross-track error. This results in a more flexible maneuvering behavior that can contribute to reaching the desired path faster as well as obtaining a diminished oscillatory behavior around the desired path. The guidance system along with a heading controller form a cascaded structure, which is shown to be κ-exponentially stable when the control task is to converge to the path produced by the aforementioned CHSI method. In addition, the issue of compensating for the sideslip angle β is discussed and a new κ-exponentially stable integral LOS guidance law, capable of eliminating the effect of constant external disturbances for straight-line path following, is derived.**

Index Terms— **Cascaded systems, constant environmental forces, integral line-of-sight (LOS) guidance, monotone cubic Hermite interpolation, time-varying lookahead distance.**

I. Introduction

GUIDANCE systems are of critical importance for the overall performance of autonomous vehicles, aircraft, marine craft, and robotic systems because they are concerned with the transient motion behavior associated with the achievement of motion control objectives (see also [1]). Path-following is one of the typical control scenarios in the control literature and it pertains to following a predefined path independent of time, i.e., without imposing any restrictions on the temporal propagation along the path. Readers interested in motion control scenarios and guidance laws may refer to [2] and [3]. At this point, it is possible to distinguish between two separate but, as we will see later on, interrelated problems: 1) the path-planning problem and 2) the guidance system design problem.

As the name indicates, path-planning pertains to the procedure of determining, which route to take when moving from one location to another. In many applications, the first step is to introduce a given order of fixed points in space, namely the waypoints, and define the desired path as the sum of the successive straight lines that connect these waypoints. Due to physical constraints though, it is not possible to achieve a smooth transition between two straight lines because, in the general case, such a path has a discontinuous first derivative (and thus velocity function) at the locations of the waypoints. This problem can be avoided by considering a straight-line path between the waypoints, as before, but with turning now being achieved by inscribing a circle between the two lines to form a curved path [4, Ch. 10]. Note that in this case, the vehicle will not pass through the waypoints and this might be an undesired effect, especially if the exact location of the waypoints has been chosen so as, for example, to avoid obstacles. It is therefore reasonable to assume that if the succession between a straight line and a circular arc (or vice versa) occurs in a way such that the final path passes through all the waypoints, both the aforementioned requirements (velocity continuity and passing through the waypoints) could be satisfied. Paths consisting of straight lines and circular arcs have been studied extensively in the past. According to Dubins's well-known result for a particle with unity speed, the shortest possible path that meets a maximum curvature bound between a starting position with predefined orientation (starting pose) and a finishing position with predefined orientation (finishing pose) consists of at most three pieces, each of which is either a straight line or an arc of a circle of radius $R > 0$ [5]. Dubins's work dealt with forward motion of car-like vehicles only, but his result was later extended by Reeds and Shepp [6] to consider backward motion as well, thus allowing to include cusps along the path. Note that, depending on the application, it is not always possible to find a Dubins path, as it was shown in [7]. Extensions of Dubins paths for satisfying curvature constraints in 3-D space have also been developed. Such a methodology was presented in [8] where a nonlinear controller resembling the LOS guidance law was employed for tracking the 3-D Dubins path.

The concatenation of straight and circular segments, however, leads to difficult transition maneuvers between these segments. This problem stems from the fact that a straight line

A. M. Lekkas is with the Centre for Ships and Ocean Structures, Norwegian University of Science and Technology, Trondheim 7491, Norway (e-mail: anastasios.lekkas@itk.ntnu.no).

T. I. Fossen is with the Department of Engineering Cybernetics, Norwegian University of Science and Technology, Trondheim 7491, Norway (e-mail: fossen@ieee.org).

has a curvature $\kappa = 0$, whereas a circle arc has a curvature $\kappa = 1/R$. Hence, there will be a jump in the curvature from 0 to $1/R$ when moving from the straight line to the circle arc. Thus, a sudden change in lateral acceleration will occur and this will lead to deviations from the desired path. This problem was tackled in [9], where continuous curvature paths with a upper-bounded derivative were designed and [10] proceeded further by considering an upper-bounded curvature, forward and backward motions and collision avoidance. The latter approach computed paths that consisted of straight segments, circular and clothoid arcs. These techniques assume car-like vehicles with models simpler than those used to describe the motion of marine vessels or airplanes, due to the lack of sway motion.

Paths of continuous curvature can also be produced using other methods. Two of the most popular approaches are the clothoid arcs and the Pythagorean hodographs (PH). The former pertains to paths composed by segments that have equal curvature at their boundaries. Paths based on clothoids consist of straight and arc segments, just like the Dubins path, but the arc segment is now computed with the help of Fresnel integrals instead of being a circular arc. The outcome is a curve with a linearly varying curvature over the path length. The latter approach results in a piecewise-polynomial path by employing polynomials of the fifth degree [11]. PH produces a flexible path with the possibility of introducing an inflection point between the two waypoints. Moreover, the path length calculation problem has a closed-form solution, contrary to what is the case with splines in general. Further work has been done in [12] so as to guarantee that the curvature constraints are satisfied as well. The main drawback of these approaches is the increased computational complexity, which can be a heavy burden when implementing them in unmanned vehicles applications, for instance. For a more detailed treatment of the design of Dubins paths, clothoid arcs, and PH, the reader is referred to [13, Ch. 2 and 3]. Following the same line of reasoning as the clothoid, the feasibility of constructing paths consisting of straight lines and Fermat's spiral arc segments was studied in [14]. It was shown that Fermat's spiral can be used to generate G^2 (curvature-continuous) paths with a very low computational cost compared with clothoids. The approach was further extended in [15] where an alternative parametrization of Fermat's spiral was proposed, hence leading to C^2 paths suitable for path tracking.

Spline interpolation techniques have also been studied extensively in the path-planning literature and, as it is expected, depending on the method chosen the resulting path can have different properties. Bezier curves, for instance, and their generalizations (B-splines) can give paths of continuous curvature but without passing through all the data points used to define it [16]. Natural splines, on the other hand, pass through the waypoints and also produce curvature-continuous paths, but do not possess local control (this refers to the case where relocating one waypoint induces changes throughout a larger part of the path) and the resulting paths are not very practical [4, Ch. 10]. An interesting alternative is the cubic Hermite spline interpolation (CHSI), which passes through all the waypoints and it is possible to assign the derivative values at the control points and also obtain local control over the path.

It should be mentioned that path-planning is a problem that has been studied extensively in the literature from several different angles and several other approaches have been developed to obtain more sophisticated trajectories. Such is the case in [17], where the authors combined the methodologies presented in [18] and [19] and developed a path-planning strategy, which smooths an optimal sequence of waypoints in 3-D space using a highly accurate nonlinear vehicle model, which is based on motion primitives. Moreover, a core paths graph, which aimed at generating optimal flight trajectories that satisfy mission constraints resulting from no-fly zones or obstacles was presented in [20]. In [21], the C^2 path generation methodology of [14] and [15] was used in combination with the Voronoi diagrams and resulted in curvature-continuous paths while achieving obstacle avoidance.

In addition to the path-planning problem, it is of great importance to implement a guidance algorithm that will steer the vehicle in a way such that it stays on the path, or lead it toward the path if the cross-track error (that is, the shortest distance to the path) is nonzero. Therefore, for a vehicle with a nonzero forward velocity, the guidance system in combination with the attitude controller should result in a stable overall system to ensure convergence to the desired trajectory. This constitutes the second problem that we are tackling in this paper. Similar to the path-planning problem, there is a vast literature regarding the guidance task. Some of the most popular methods adopted by the marine community include the line-of-sight (LOS) guidance (see also [22]), the pure pursuit guidance and the constant bearing guidance, all these methods are presented in detail in [3]. Optimal methods have also appeared in the literature, for more details, the reader is referred to [23] and [24].

Healey and Lienard [25] addressed the problem of guiding an underwater vehicle with a LOS guidance algorithm and designing a sliding mode controller for stabilizing the combined speed, steering, and diving response. In [26], a guidance-based path-following scheme, which is singularity-free for all regular paths in conjunction with a nonlinear backstepping controller was presented and uniform global asymptotic stability (UGAS) and uniformly local exponential stability (ULES) was proven using cascade theory. A cascaded systems approach was also developed by [27] where the guidance system is interconnected with a sliding mode controller to achieve global κ-exponential stability to straight lines in 3-D space. The concept of κ-exponential stability implies both UGAS and ULES and was introduced in [28]. A control strategy for formation control and straight-line path following for underactuated surface vessels was developed in [29] where the cascade system formed by the closed-loop path following dynamics and the closed-loop synchronization dynamics was shown to be UGAS and ULES. In all the aforementioned approaches, a constant lookahead distance was considered. The importance of using a variable lookahead distance was demonstrated in the κ-exponentially stable guidance laws, which were developed at a kinematics level and proposed in [30]. Pavlov *et al.* [31] presented a UGAS nonlinear model predictive control (MPC) approach where the lookahead

distance, Δ, was optimized to achieve a combination of fast convergence and small overshoot compared with the constant lookahead LOS algorithms. In [32], the LOS guidance parameter was embedded in the linear MPC controller design as as additional decision variable and the simulations indicated a smoother convergence to a straight line compared with the linear MPC controller with a fixed lookahead distance. In [33], different direction was followed by proposing a time-varying lookahead distance Δ equation, which is dependent on the cross-track error. This results in lower values for Δ (and thus a more agile and aggressive response) when the vehicle is far from the desired path, and greater Δ values when the vehicle is closer to the path and less abrupt behavior is needed so as to avoid oscillating around the path. The minimum and maximum values for Δ can be determined by the user and should depend on the maneuvering characteristics of the vehicle. The method was shown to be κ-exponentially stable and the simulations of the motion of a Mariner class vessel indicated that the time-varying lookahead distance guidance algorithm can improve performance. Furthermore, several modifications have been proposed in the past so as to obtain a modified version of the LOS guidance law that can compensate for the influence of constant external disturbances, such were the integral LOS algorithms studied in [1] and [34].

This paper contributes to the path-planning problem by implementing a variation of the CHSI, which is based on the algorithm presented in [35], to produce the desired path. In this way, the path between the waypoints is generated using a monotonicity-preserving cubic interpolant and this turns out to be an effective method to address the path-planning problem, especially in the case where the waypoints are the result of a nonsmooth function. The resulting path is not continuous on the second derivative, but this problem can be alleviated by using a first-order filter before feeding the yaw rate commands to the controller. Moreover, the monotone CHSI algorithm generally gives more practical paths (by avoiding wiggles and zigzags) compared with some common curvature-continuous spline methods, natural cubic splines for instance.

Regarding the guidance problem, the contribution of this paper is the continuation of the work of [33] using a modified formula for Δ and extending the method to curved path following. A globally exponentially stable (GES) sliding mode controller is designed for stabilizing the yaw angle of the vehicle and acts as the perturbing system in the cascade system that it forms along with the well-known LOS guidance law [36], which now incorporates the time-varying look ahead distance equation. The cascade is shown to be globally κ-exponentially stable when the task is to converge to the curved path, which is constructed by the monotone version of the Hermite spline interpolation [35].

In addition to this, we present a new integral LOS algorithm capable of canceling the effects of constant (with respect to the inertial frame) environmental disturbances, such as ocean currents. The new solution is derived using simple Lyapunov analysis based on the kinematics of the vehicle's motion and computer simulations indicate that it succeeds in eliminating the cross-track error caused by the unknown ocean current.

The proposed algorithm has a small computational footprint compared with nonlinear constrained optimization methods, which require a fast computer. Therefore, it is possible to implement the path-following controller and cubic spline algorithms onboard a small autonomous vehicle using an embedded computer with limited clock frequency to reduce the energy consumption. Typical applications are path-following control systems for autonomous underwater vehicles, unmanned aerial vehicles, unmanned surface vehicles as well as conventional ships, aircraft and land-based vehicles. Simulations of the proposed method indicate that smooth convergence, without oscillations around the desired path, is achieved. Similar to [27] and [31], the combination of UGAS and ULES stability results in a robust behavior against modeling uncertainties or unmeasured external forces and disturbances.

The rest of this paper is organized as follows. In Section II, the monotone interpolation using cubic Hermite splines is presented. Section III discusses the kinematics of the vehicle as well as the control objective. Section IV presents the time-varying Δ equation and gives the stability proof of the LOS algorithm. A sliding mode controller for stabilizing the heading angle is designed in Section V. The systems' interconnection and the cascade structure is studied in Section VI. The compensation of the sideslip angle in discussed in Section VII. In Section VIII, the proposed method is tested via simulations and, finally, Section IX gives an overview of this paper and discusses future work.

II. Monotone CHSI

It is a common practice in many applications to use polynomials as a means of performing interpolation on a given data set. Given the values (also called control points) $f_1, \ldots, f_n$ of the function f at some finite set of points $\{x_1, \ldots, x_n\}$, an interpolating curve is one that passes through each point and an approximating curve is one that gets close but does not necessarily pass through all the points. For path-following applications, it is natural to require that the curve connecting the waypoints is an interpolating one, since the initial waypoint planning might have been developed with obstacle avoidance in mind. The polynomial that results in an interpolating curve is called the Lagrange interpolation polynomial. In the case where f is differentiable and the problem includes constraints related to the derivative of f at the interpolated points, the polynomial that gives the desired curve is called a Hermite interpolation polynomial. Nevertheless, for a high number of waypoints a high degree polynomial is necessary to pass through all of them. This is unwanted because the outcome would be a very intractable and of no practical use path, due to Runge's phenomenon.

Therefore, a solution to the path generation problem is to use a Hermite interpolating polynomial of degree 3 (that is, a cubic Hermite spline) for each pair of successive waypoints. Given a nonnegative integer n, let $\mathcal{P}_n$ denote the set of all real-valued polynomials of degree $\leq n$ defined over the set $\mathbb{R}$. A polynomial $p_3 \in \mathcal{P}_3$ guarantees that the velocity function is smooth between the successive waypoints and the assigned

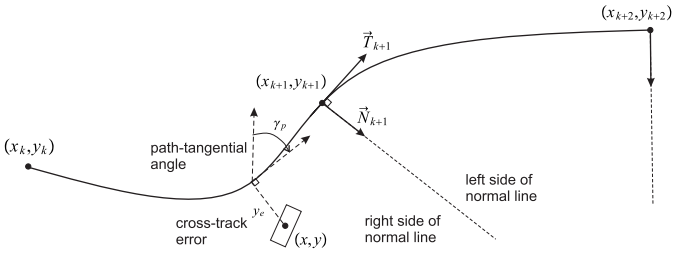

Fig. 1. Curved path-planning between waypoints.

derivative values at each waypoint ensure that the velocity function is smooth along the whole path. In addition to this, the curvature function is continuous between the successive waypoints but, in general, not continuous on the assigned waypoints. Fig. 1 illustrates the geometry of a curved path between waypoints.

Following [35], we define $\pi : a = x_1 < x_2 < \cdots < x_n = b$ as a partition of the interval $I = [a, b]$ and $f_i : i = 1, 2, \ldots, n$ the corresponding set of monotone data at the partition points (also knots, or control points). The algorithm of Fritsch and Carlson constructs on π a piecewise cubic function $p(x_i) \in C^1[I]$ such that

$$p(x_i) = f_i \;\; i = 1, 2, \ldots, n \tag{1}$$

and $p(x)$ is monotone. In each subinterval $I_i = [x_i, x_{i+1}]$, $p(x)$ is a cubic polynomial, which can be described by

$$p(x) = f_i H_1(x) + f_{i+1} H_2(x) + d_i H_3(x) + d_{i+1} H_4(x) \tag{2}$$

with $d_j = p'(x_j)$ denoting the corresponding first derivatives at the points $j = i,\ i + 1$ and the terms $H_k(x)$ are the cubic Hermite basis functions for the interval I_i

$$\begin{aligned} H_1(x) &= \zeta((x_{i+1} - x)/h_i) \\ H_3(x) &= -h_i \eta((x_{i+1} - x)/h_i) \\ H_2(x) &= \zeta((x - x_i)/h_i) \\ H_4(x) &= h_i \eta((x - x_i)/h_i) \end{aligned} \tag{3}$$

where $h_i = x_{i+1} - x_i$, $\zeta(t) = 3t^2 - 2t^3$, $\eta(t) = t^3 - t^2$. To preserve monotonicity, the algorithm adjusts the tangents at the control points in the following way [37].

Let $S_i = (f_{i+1} - f_i)/h_i$ be the slopes of the piecewise linear interpolants. Therefore, if S_i and S_{i-1} have opposite signs, or either of them is zero, this means that x_i is a local minimum or maximum and therefore we set

$$d_i = 0. \tag{4}$$

In the case where S_i and S_{i-1} have the same sign and the corresponding intervals are of the same length, then the tangent is calculated as

$$\frac{1}{d_i} = \frac{1}{2}\left(\frac{1}{S_{i-1}} + \frac{1}{S_i}\right). \tag{5}$$

Finally, if S_i and S_{i-1} have the same sign but the corresponding intervals have different length, we calculate the tangent as

$$\frac{w_1 + w_2}{d_i} = \frac{w_1}{S_{i-1}} + \frac{w_2}{S_i} \tag{6}$$

where $w_1 = 2h_i + h_{i-1}$, $w_2 = h_i + 2h_{i-1}$. The algorithm is also available in MATLAB (function pchip.m).

The methodology described above can be extended to parametric splines. This entails the introduction of the independent variable θ and the formulation of one separate equation for each one of the data variables $(x, f(x)) = (x, y)$. Let $\theta_1 < \theta_2, \ldots, \theta_n$ be the path variable or partition of the interval $[\theta_1, \theta_n]$, and let (x_i, y_i) for $i = 1, 2, \ldots, n$ be the corresponding 2-D waypoints. Based on [35], we can interpolate the data between two waypoints (x_i, y_i) and (x_{i+1}, y_{i+1}) according to

$$x_d(\theta) = c_{x3}(\theta - \theta_i)^3 + c_{x2}(\theta - \theta_i)^2 + c_{x1}(\theta - \theta_i) + c_{x0} \tag{7}$$

$$y_d(\theta) = c_{y3}(\theta - \theta_i)^3 + c_{y2}(\theta - \theta_i)^2 + c_{y1}(\theta - \theta_i) + c_{y0} \tag{8}$$

where

$$\begin{aligned} c_{x0} &= x_i & c_{y0} &= y_i \\ c_{x1} &= x_i' & c_{y1} &= y_i' \\ c_{x2} &= \frac{3S_i^x - x_{i+1}' - 2x_i'}{\Delta\theta_i} & c_{y2} &= \frac{3S_i^y - y_{i+1}' - 2y_i'}{\Delta\theta_i} \\ c_{x3} &= \frac{x_{i+1}' + x_i' - 2S_i^x}{\Delta\theta_i^2} & c_{y3} &= \frac{y_{i+1}' + y_i' - 2S_i^y}{\Delta\theta_i^2} \end{aligned} \tag{9}$$

with $(\cdot)'$ denoting differentiation with respect to parameter θ, $\Delta\theta_i = \theta_{i+1} - \theta_i$ is the local mesh spacing, and $S_i^x = (x_{i+1} - x_i)/\Delta\theta_{i+1}$ and $S_i^y = (y_{i+1} - y_i)/\Delta\theta_{i+1}$ are the slopes of the piecewise linear interpolants.

A. Discussion Regarding the Curvature

When it comes to path generation methods, there are two main concerns related to the curvature: 1) whether the method is curvature-continuous or not and 2) if is it possible to assign a maximum curvature throughout the path. In accordance with the nonparametric case, the interpolants have continuous derivatives, $x_d(\theta) \in C^1$ and $y_d(\theta) \in C^1$, but not necessarily a continuous second derivative. The continuity of the second derivative and the order of accuracy depend on how x_i' and y_i' are calculated. Therefore, the CHSI is, in the general case, discontinuous on the locations of the waypoints. This affects the heading controller input and is further discussed in Section IV. In addition to this, and despite the fact that splines have a closed-form expression of position, assigning maximum curvature to a planar path generated by parametric polynomial cubic curves has been reported to be a difficult problem, see for instance [38] and [39]. The reason for this is that the curvature of such a parametric curve is a complicated function of the curve's parameters. The CHSI has been employed in this paper to: 1) prove stability of the time-varying lookahead distance LOS guidance when converging to curved paths (see Section IV) and 2) demonstrate the partial/local control property of paths (Section VIII), which can be useful for real-time applications.

III. Vehicle Model and Control Objective

A. Vehicle Model

The North-East-Down (NED) coordinate system $\{n\} = (x_n, y_n, z_n)$ and the body-fixed reference frame $\{b\} = (x_b, y_b, z_b)$ will be used in this paper to describe the motion, location, and orientation of the vehicle. The NED

frame is defined as a tangent plane on the surface of the Earth moving with the vehicle and is sufficient for local operations. Its origin is o_n and the x-axis points toward the true North, the y-axis points toward the true East and the z-axis points downward, normal to the Earth's surface. The body-fixed frame is moving with the vehicle and its origin o_b coincides with the center of gravity of the vehicle, see also [4, Ch. 2]. Consider a surface vehicle at the position (x, y) moving with the speed

$$U = \sqrt{u^2 + v^2} \tag{10}$$

where u and v are the velocities in surge and sway, respectively. The speed U is assumed to be positive and bounded

$$U_{\min} \leq U \leq U_{\max}, \quad 0 < U_{\min}. \tag{11}$$

The three degree-of-freedom (DOF) horizontal dynamics of the surface vehicle can be represented by three differential equations

$$\dot{u} = f_u(u, v, r, \tau) \tag{12}$$
$$\dot{v} = f_v(u, v, r, \tau) \tag{13}$$
$$\dot{r} = f_r(u, v, r, \tau) \tag{14}$$

where $\dot{(\cdot)}$ denotes differentiation with respect to time and τ is the vector of the control forces and moments generated by the actuators. The kinematic equations are

$$\dot{x} = u\cos(\psi) - v\sin(\psi) \tag{15}$$
$$\dot{y} = u\sin(\psi) + v\cos(\psi) \tag{16}$$
$$\dot{\psi} = r \tag{17}$$

where ψ is the yaw angle relative to the NED reference frame (true North) and r is the yaw rate of the vehicle. The model (15)–(17) describes the motion of an underactuated vehicle since two out of three DOFs can be controlled independently, namely the yaw angle and the surge velocity. In this paper, we are dealing with only the path-following task, which (following the definition given in [40]) does not impose temporal restrictions and therefore we assume that the speed is measured and manually controlled, hence the speed control problem will not be addressed. Furthermore, (15)–(17) assume that there are no environmental forces acting on the system and thus ignore the relative velocities that would appear as a result of the vehicle's motion with respect to the wind or ocean currents. This assumption will be relaxed in Section VII.

B. Control Objective

The minimum distance between the vehicle and the monotonic curve between the two waypoints will be used as cross-track error. Since the vehicle moves with speed U, the position (x, y) of the vehicle will be time-varying. Hence, an analytical expression for the cross-track error will be derived such that the LOS path-following controller can minimize the path error. Differentiation of the Hermite interpolants (7) and (8) with respect to the parameter θ gives the first derivatives

$$x_d'(\theta) = 3c_{x3}(\theta - \theta_i)^2 + 2c_{x2}(\theta - \theta_i) + c_{x1}\theta \tag{18}$$
$$y_d'(\theta) = 3c_{y3}(\theta - \theta_i)^2 + 2c_{y2}(\theta - \theta_i) + c_{y1}\theta \tag{19}$$

and the second derivatives

$$x_d''(\theta) = 6c_{x3}(\theta - \theta_i) + 2c_{x2} \tag{20}$$
$$y_d''(\theta) = 6c_{y3}(\theta - \theta_i) + 2c_{y2}. \tag{21}$$

The tangent and normal lines through the point $(x_d(\theta), y_d(\theta))$ are given by

$$y_t - y_d(\theta) = \frac{y_d'(\theta)}{x_d'(\theta)}(x_t - x_d(\theta)) \tag{22}$$
$$y_n - y_d(\theta) = -\frac{1}{\frac{y_d'(\theta)}{x_d'(\theta)}}(x_n - x_d(\theta)). \tag{23}$$

The θ value corresponding to the path-normal that intersects the vehicle is found by requiring that $(x_n, y_n) = (x, y)$. Moreover, from (23) it follows that:

$$y_d'(\theta^*)(y - y_d(\theta^*)) + x_d'(\theta^*)(x - x_d(\theta^*)) = 0. \tag{24}$$

This involves solving the roots of the third-order cubic function for θ^*. Instead of using an analytical solution a numerical solution based on Newton–Raphson method will converge quite fast. For instance

$$\theta_{j+1}^* = \theta_j^* - \frac{f(\theta_j^*)}{f'(\theta_j^*)} \tag{25}$$

with

$$f(\theta_j^*) = y_d'(\theta_l^*)(y - y_d(\theta_j^*)) + x_d'(\theta_j^*)(x - x_d(\theta_j^*)) \tag{26}$$
$$f'(\theta_j^*) = y_d''(\theta_j^*)(y - y_d(\theta_j^*)) + x_d''(\theta_j^*)(x - x_d(\theta_j^*)) - x_d'(\theta_j^*)^2 - y_d'(\theta_j^*)^2 \tag{27}$$

will converge in a few iterations if the initial path variable θ_0^* is taken as the last θ_i value when moving along the path between two waypoints parameterized on the interval $[\theta_1, \theta_n]$. In this paper, we do not deal with the singularity that might occur when the vehicle's position is projected on the path, which is when the path consists of circular arc segments, for instance. There have been efficient solutions for this problem in the literature, which are easy to implement, for more details see [41] and [42].

The normal line from the point $(x_d(\theta^*), y_d(\theta^*))$ on the path through the point (x, y) on the vehicle defines the along- and cross-track errors (x_e, y_e). Moreover

$$\begin{bmatrix} x_e \\ y_e \end{bmatrix} = \mathbf{R}^\top(\gamma_p) \begin{bmatrix} x - x_d(\theta^*) \\ y - y_d(\theta^*) \end{bmatrix} \tag{28}$$
$$\mathbf{R}(\gamma_p) = \begin{bmatrix} \cos(\gamma_p) & -\sin(\gamma_p) \\ \sin(\gamma_p) & \cos(\gamma_p) \end{bmatrix} \tag{29}$$

where $\mathbf{R}(\gamma_p) \in SO(2)$ is the rotation matrix in yaw. In algebraic form, the equations of the along- and the cross-track error for a given vehicle position (x, y) become

$$x_e = (x - x_d(\theta^*))\cos(\gamma_p) + (y - y_d(\theta^*))\sin(\gamma_p) \tag{30}$$
$$y_e = -(x - x_d(\theta^*))\sin(\gamma_p) + (y - y_d(\theta^*))\cos(\gamma_p) \tag{31}$$

where γ_p is the path-tangential angle

$$\gamma_p = \text{atan2}(y_d'(\theta^*), x_d'(\theta^*)) \tag{32}$$

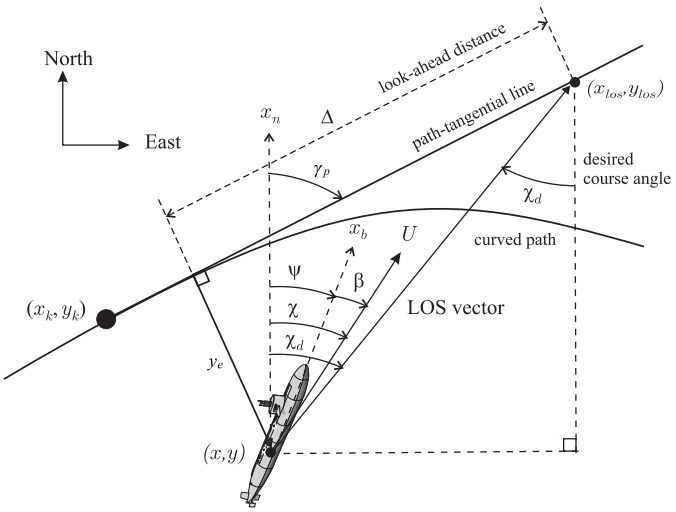

Fig. 2. LOS guidance geometry for curved paths.

and the two-argument function atan2 is a generalization of the $\arctan(y/x)$ that takes into account the signs of both x and y to determine the quadrant of the result, hence making it possible to distinguish between diametrically opposite directions.

Finally, the associated control objective for curved path-following is:

$$\lim_{t\to+\infty} y_e(t) = 0. \tag{33}$$

Note that in the case where temporal constraints are needed (for example, in a path- or target-tracking scenario) then it is necessary to include the along-track error dynamics in our study as well.

IV. Time-Varying Lookahead Distance Guidance Law

A. LOS Guidance Law

Fig. 2 shows the geometry of the LOS guidance problem and some of the main variables that are involved in it. Before moving on, it is useful to mention that the LOS vector is often defined differently in marine applications compared with the definition adopted by the aircraft and missile communities. According to the definition in [2], the LOS is the line that starts at the reference point (that is, the aircraft or the missile) and passes through the objective of the guidance, i.e., the target. On the other hand, in marine guidance applications the LOS vector starts at the vessel and passes through a point $\mathbf{p}(x_{\text{los}}, y_{\text{los}})$, which is located on the path-tangential line at a lookahead distance $\Delta(t) > 0$ ahead of the direct projection of the vessel's position $\mathbf{p}(x, y)$ on to the path. In this paper, the lookahead-based steering method will be considered. The corresponding guidance law is given by

$$\chi_d = \gamma_p + \arctan\left(\frac{-y_e}{\Delta}\right) \tag{34}$$

where χ_d is the desired course angle of the vehicle

$$\chi_d = \psi_d + \beta \tag{35}$$

where β is the sideslip angle of the vehicle. These variables will be explained in more detail in Section VII. In other words, the LOS guidance ensures that the vehicle's velocity is directed toward the moving point $\mathbf{p}(x_{\text{los}}, y_{\text{los}})$ until the vehicle converges to the path, which indicates that the control objective (33) has been satisfied.

By differentiating (31) with respect to time, we get

$$\begin{aligned}\dot{y}_e &= -(\dot{x} - \dot{x}_d(\theta^*))\sin(\gamma_p) - (x - x_d(\theta^*))\cos(\gamma_p)\dot{\gamma_p} \\ &\quad +(\dot{y} - \dot{y}_d(\theta^*))\cos(\gamma_p) - (y - y_d(\theta^*))\sin(\gamma_p)\dot{\gamma_p} \\ &= \underbrace{u\sin(\psi - \gamma_p) + v\cos(\psi - \gamma_p)}_{n_1} \\ &\quad + \underbrace{\dot{x}_d(\theta^*)\sin(\gamma_p) - \dot{y}_d(\theta^*)\cos(\gamma_p)}_{n_2} \\ &\quad -\dot{\gamma_p}\underbrace{((x - x_d(\theta^*))\cos(\gamma_p) + (y - y_d(\theta^*))\sin(\gamma_p))}_{\text{Along-track distance } x_e}.\end{aligned} \tag{36}$$

The sums n_1 and n_2 can be transformed in amplitude-phase form, consequently we obtain

$$n_1 = \sqrt{u^2 + v^2}\sin(\psi - \gamma_p + \beta) \tag{37}$$

where

$$\beta = \text{atan2}(v, u) \tag{38}$$

which is equal to the orientation of the vehicle's velocity vector $U(u, v)$ with respect to the body-fixed frame. In other words, (38) is the angle between the vehicle's velocity orientation and the vehicle's heading. This is the commonly known as sideslip, or drift, angle.

The second term can be rewritten as

$$n_2 = \dot{\theta}\sqrt{x'(\theta)^2 + y'(\theta)^2}\sin(\gamma_p + \phi) \tag{39}$$

where

$$\phi = \text{atan2}(-y'(\theta), x'(\theta)) \tag{40}$$

$$= -\gamma_p. \tag{41}$$

From (39) and (41), we conclude that $n_2 = 0$. Regarding the along-track error, x_e, we can conclude from (23) that

$$(y - y_d) = -\frac{1}{\tan(\gamma_p)}(x - x_d) \Rightarrow \tag{42}$$

$$x_e = 0 \tag{43}$$

and consequently

$$\dot{y}_e = U\sin(\psi - \gamma_p + \beta). \tag{44}$$

If we assume that the desired heading is perfectly tracked at all times and choose the desired heading angle as

$$\psi_d = \gamma_p + \arctan\left(\frac{-y_e}{\Delta}\right) - \beta \tag{45}$$

the derivative of the cross-track error becomes

$$\dot{y}_e = U\frac{-y_e}{\sqrt{\Delta^2 + y_e^2}}. \tag{46}$$

The aforementioned assumption is not an oversimplification because the overall system (i.e., the guidance system and the

heading controller) will be analyzed as a cascade structure where (44) constitutes the nominal system Σ_1 and the heading error dynamics constitutes the perturbing (or driving) system Σ_2. Therefore, the stability analysis will show whether the time that the controller needs to converge can have a destabilizing effect on the guidance system. This will be further explained later on.

The Lyapunov function candidate (LFC) $V_1 = (1/2)y_e^2$ has the time-derivative

$$\dot{V}_1 = U\frac{-y_e^2}{\sqrt{\Delta^2 + y_e^2}}. \tag{47}$$

which is negative definite since $U > U_{\min}$. Hence, the origin $y_e = 0$ is a UGAS equilibrium of the nominal system Σ_1. Moreover, on the ball $D = \{y_e \in R | y_e| \leq \mu\}$, $\mu > 0$, we have that

$$\dot{V}_1 = -\frac{Uy_e^2}{\sqrt{\mu^2 + \Delta^2}} \leq -ky_e^2 \tag{48}$$

for some $0 < k < U/(\sqrt{\mu^2 + \Delta^2})$, which entails that the origin is a ULES equilibrium. The combination of UGAS and ULES implies global κ-exponential stability, according to [43].

B. Time-Varying Lookahead Distance

So far in our analysis, we have considered a constant lookahead distance Δ. If we neglect, temporarily, the path-tangential angle γ_p and focus on the part of the LOS guidance that is a function of Δ, we can write

$$\chi_r = \arctan(-K_p y_e) \tag{49}$$

with $K_p = 1/\Delta$, which implies that the lookahead-based steering guidance law is equivalent to a saturated proportional control law [4, Ch. 10]. Moreover, as it can be deduced from Fig. 2, more aggressive steering will occur for a lower Δ value compared with a greater one. This fact motivates us to propose the following formula for the lookahead distance:

$$\Delta(y_e) = (\Delta_{\max} - \Delta_{\min})e^{-K_\Delta y_e^2} + \Delta_{\min} \tag{50}$$

where $\Delta_{\min}$ and $\Delta_{\max}$ are the minimum and maximum allowed values for Δ, respectively and, along with the convergence rate $K_\Delta > 0$, constitute the design parameters. The idea behind (50) is intuitive and simple and it can be summarized by the fact that a small Δ value is assigned when the vehicle is far from the desired path, (thus resulting in a more aggressive behavior that tends to decrease the cross-track error faster) and a large value for Δ is assigned when the vehicle is close to the path and overshooting needs to be avoided. The concepts far and close with respect to the desired trajectory are relative and the designer should take several considerations into account when determining $\Delta_{\min}$, $\Delta_{\max}$, and K_Δ, such as the maneuvering characteristics of the vehicle. For the sake of notational brevity, we assign $\Delta_r := \Delta_{\max} - \Delta_{\min}$ and $\Delta := \Delta(y_e)$. In [33] we proposed a formula for $\Delta(y_e)$, which is slightly different than (50) since it included the absolute value instead of the square of the cross-track error. However, the time-derivative of Δ is required when designing the vehicle's heading controller and this can be the reason for a nonsmooth controller input. Adopting (50) circumvents this problem.

1) How the Time-Varying Δ Affects the Stability Properties of the Guidance System: Equation (48) can now be rewritten as

$$\dot{V}_1 = -\frac{Uy_e^2}{\sqrt{\mu^2 + \Delta_{\max}^2}} \leq -ky_e^2. \tag{51}$$

From (51), we see the effect of the variable lookahead formula on the stability properties of the guidance system, compared with what would have been the case with a constant Δ. More specifically, the region where the guidance system is ULES is constrained by $\Delta_{\max}$. Therefore, the larger $\Delta_{\max}$ is, the more limited the region where the system is ULES becomes.

V. Heading Autopilot Design

In this section, the stability of the vehicle's heading dynamics with the aid of a sliding mode controller is presented. To describe the yaw dynamics (14) of a marine craft, the nonlinear extension of Nomoto's first-order model [44] is considered

$$T\dot{r} + H_N(r) = K\delta \tag{52}$$

$$H_N(r) = n_3 r^3 + n_2 r^2 + n_1 r + n_0 \tag{53}$$

where r is the yaw rate, δ the rudder control input, T and K the Nomoto time and gain constants, respectively, and $H_N(r)$ is a nonlinear function describing the maneuvering characteristics of the ship. For a course stable craft $n_1 > 0$, $T, K > 0$ and assuming symmetry in the hull implies $n_2 = 0$. The bias term n_0 can be treated as an additional rudder offset in the case where a constant rudder angle is required to compensate for constant environmental forces. Therefore, a large number marine of craft can be described by

$$\dot{r} + \alpha_1 r^3 + \alpha_2 r = b\delta \tag{54}$$

where $\alpha_1 = n_3/T > 0$, $\alpha_2 = n_1/T > 0$, and $K/T = b > 0$. Equivalently, in state-space form

$$\dot{r} = -\alpha_1 r^3 - \alpha_2 r + b\delta \tag{55}$$

$$\dot{\psi} = r. \tag{56}$$

This formulation is a simplification compared with a real ship. In reality, the rudder input often does not affect the dynamics linearly and the Nomoto coefficients change as a function of the forward ship speed. Equations (55) and (56) constitute the perturbing system Σ_2. To control the system (55) and (56), we will construct a sliding mode controller. As mentioned before, the goal is to stabilize the heading angle at the desired value (45), consequently the desired heading rate can be computed as follows:

$$r_d = \dot{\psi}_d = \frac{\Delta^2}{\Delta^2 + y_e^2}\left(\frac{-\dot{y}_e}{\Delta}\right) + \dot{\gamma_p} - \dot{\beta}. \tag{57}$$

Assuming that the reference signals ψ_d, r_d are smooth, we define the sliding surface

$$s := \bar{r} + \lambda\bar{\psi} \tag{58}$$

where

$$\bar{\psi} = \psi - \psi_d, \qquad \bar{r} = r - r_d \tag{59}$$

and $\lambda > 0$ is a design parameter reflecting the bandwidth of the controller. Next, we propose the LFC $V_2 = (1/2)s^2$ and by differentiating along the trajectories of s, we get

$$\dot{V}_2 = s(-\alpha_1 r^3 - \alpha_2 r + b\delta - \dot{r}_d + \lambda \bar{r}). \tag{60}$$

Consequently, the control law

$$\delta = (1/b)(\alpha_1 r^3 + \alpha_2 r + \dot{r}_d - \lambda \bar{r} - k_d s - k_s \text{sgn}(s)) \tag{61}$$

with $k_d > 0,\ k_s \geq 0$ gives

$$\dot{V}_2 = -k_d s^2 - k_s |s| \leq -k_d s^2. \tag{62}$$

Therefore, the equilibrium point $s = 0$ is GES . From (58), it follows that $\bar{\psi} = 0,\ \bar{r} = 0$ are also GES equilibria, [45], [46]. It should be noted that autopilots can be sensitive to parametric uncertainty and unmodeled dynamics, hence the inclusion of the sliding mode term $k_s \text{sgn}(s)$ in (62).

2) Discussion on the Continuity of the Reference Signals: As it was shown in Section II, the CHSI does not result in paths with continuous second derivative due to the discontinuities that occur at the waypoint locations. Given the fact that the curvature of a parameterized curve $\mathbf{r}(\theta) = (x(\theta), y(\theta))$ is calculated as

$$\kappa_r = \frac{x'y'' - x''y'}{(x'^2 + y'^2)^{3/2}} \tag{63}$$

and the lateral acceleration a_L of the vehicle can be computed as

$$a_L = U^2 \kappa_r \tag{64}$$

we can easily conclude that, in the general case, there will be a step in the desired lateral acceleration of the vehicle when passing through a waypoint. This can also be verified by the desired heading rate (57), which inherently is a function of the path's second derivative via the term $\dot{\gamma}_p$. Thus, ψ_d is always a continuous signal but the same is not true for r_d. For vehicles with low turning rates, such as marine craft, it is not critical to include r_d in the controller and, thus, setting $r_d = 0$ will not affect the performance significantly. This will be demonstrated by simulating accordingly in Section VIII. For highly accelerated vehicles, however, it is recommended to use a filter before feeding the heading rate to the controller, or, alternatively, use a different parametrization.

VI. Interconnection Between the Guidance System and the Heading Autopilot

The two nonlinear systems (46) and (55) and (56) are interconnected and form a cascade structure. The driving system is the sliding mode controller since the convergence to the desired yaw angle ψ_d affects the stability of the guidance system via the state $\bar{\psi} = \psi - \psi_d$. However, the guidance system perturbs the yaw control system as well, not only via the desired yaw angle ψ_d but also because the cross-track error appears in the desired heading rate equation. This implies that apart from the three assumptions that need to be satisfied to infer upon the stability of the cascade system (for the theoretical background and the proofs of the related theorems the reader is referred to [47]), it is necessary to prove that the system is forward complete.

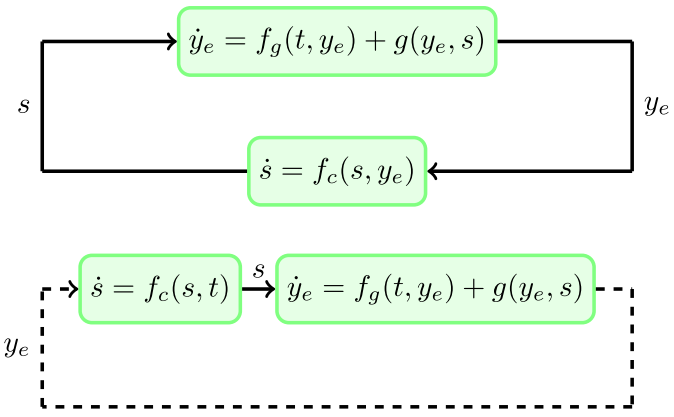

Fig. 3. Equivalence between the closed-loop system and the cascade structure. This holds because the closed-loop system is forward complete.

A system is called forward complete if for every initial condition r and every input signal u, the corresponding solution is defined for all $t \geq 0$, i.e., $\sigma^{\max_{r,u}} = +\infty$ [48]. We achieve this in a similar manner as in [49], but before proceeding with the proof we compute the interconnecting term

$$\begin{aligned} g(y_e, s) &= U(\sin(\psi - \gamma_p) - \sin(\psi_d - \gamma_p)) \\ &= 2U \sin\left(\frac{\bar{\psi}}{2}\right) \cos\left(\gamma_p - \frac{\psi + \psi_d}{2}\right). \end{aligned} \tag{65}$$

Equation (65) shows how the heading error dynamics acts and prevents $U \sin(\psi - \gamma_p)$ from becoming equal to $U \sin(\psi_d - \gamma_p)$ instantaneously. Obviously, if at each time instant, we had $\psi = \psi_d \ \Rightarrow \ \bar{\psi} = 0$, then $g(y_e, s) = 0\ \forall t$. But this perfect heading tracking scenario is never possible in reality due to the yaw inertia of the vehicle, hence the cascaded nature of the overall system.

A. Forward Completeness of the Closed-Loop System

Equation (65) allows the two systems (46) and (55) and (56) to be rewritten as follows:

$$\Sigma_1 : \dot{y}_e = f_g(t, y_e) + g(y_e, s) \tag{66}$$

$$\Sigma_2 : \dot{s} = f_c(y_e, s) \tag{67}$$

where $f_g(t, y_e) = U \sin(\psi_d - \alpha)$. By proving that (92) and (93) is forward complete, we can consider $f_c(s, y_e)$ to be a time-varying function so as $f_c(s, y_e) = f_c(s, t)$

$$\Sigma_1 : \ \dot{y}_e = f_g(t, y_e) + g(y_e, s) \tag{68}$$

$$\Sigma_2' : \ \dot{s} = f_c(s, t) \tag{69}$$

This equivalence is shown in Fig. 3. Then, it is possible to use the theorems from [47].

According to [48], if a system is forward complete, then there exist a nonnegative, radially unbounded, smooth function $V : \mathbb{R}^n \to \mathbb{R}_+$ and a class-$\mathcal{K}_\infty$ function σ such that

$$\frac{\partial V(x)}{\partial x} f(x, u) \leq V(x) + \sigma(|u|) \tag{70}$$

$\forall\ x \in \mathbb{R}^n$ and $\forall\ u \in \mathbb{R}$. To show that the system (92) and (93) is forward complete, we employ the LFC

$$V_{fc} = \frac{1}{2} y_e^2 + \frac{1}{2} s^2 \tag{71}$$

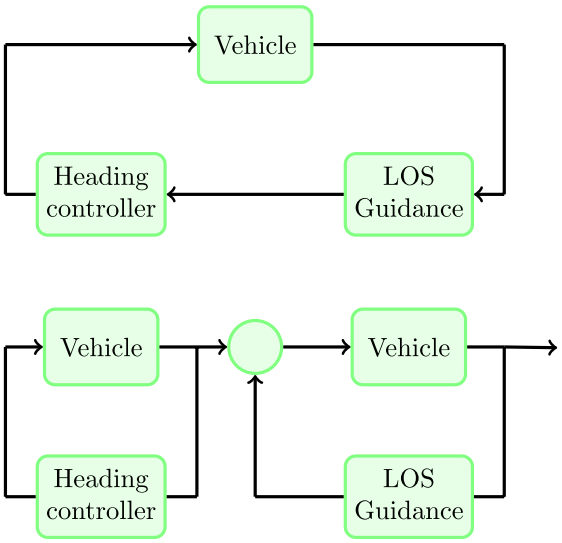

Fig. 4. Overall system is a cascade where the vehicle along with the heading controller is the driving system Σ_2' and the vehicle in combination with the LOS guidance constitutes the driven system Σ_1. The yaw angle tracking error affects the convergence of the guidance system's objective, which is to minimize the cross-track error.

which gives

$$\frac{\partial V_{fc}}{\partial x} f(x,u) = -\frac{U y_e^2}{\sqrt{y_e^2+\Delta^2}} + g(y_e,s) y_e - k_d s^2. \quad (72)$$

The first and third terms of the right-hand side of the equation are negative. Regarding $g(y_e, s)$, from (65), we can write

$$g(y_e,s) \leq 2U_{\max}. \quad (73)$$

Therefore, (72) becomes

$$\frac{\partial V_{fc}}{\partial x} f(x,u) \leq V_{fc} + 2U_{\max}|y_e|. \quad (74)$$

Hence, we have shown that the system is forward complete. This result implies that we can proceed and analyze the overall system as a cascaded system. This fact leads to a separation principle, the structure of which can be observed in Fig. 4.

B. Stability of the Cascade Structure

We choose the state vector that contains the error states of both the control and guidance systems that form the cascade

$$\mathbf{x} = [y_e, \bar{\psi}, \bar{r}]^{\mathrm{T}} \quad (75)$$

Hence we continue by stating the following theorem.

Theorem 1 (K-Exponentially Stable Cascade): The origin $\mathbf{x} = \mathbf{0}$ of the cascade structure (68) and (69) [formed by the perturbing system (55) and (56) and the perturbed system (46)] is globally κ-exponentially stable if the control law is given by (61), and the desired yaw angle is described by (45).

Proof: The proof consists of showing that the three assumptions of Theorem 1 in [47] are satisfied. In this paper, however, we will also use the formulation given in [50] to prove global κ-exponential stability.

Assumption A1: We already showed that the equilibrium point $y_e = 0$ is globally κ-exponentially stable. We also have that $V_1 = (1/2)y_e^2$, and

$$\left|\frac{\partial V_1}{\partial y_e}\right| |y_e| = |y_e||y_e|$$
$$\Rightarrow \left|\frac{\partial V_1}{\partial y_e}\right| |y_e| \leq c_1 V_1(y_e) \quad \text{for} \quad c_1 \geq 2 \quad \text{and} \quad \forall |y_e| \geq 0. \quad (76)$$

The condition

$$\left|\frac{\partial V_1}{\partial y_e}\right| \leq c_2 \quad \forall |y_e| \leq \mu \quad (77)$$

is also satisfied $\forall |y_e| \leq \mu, \quad \mu > 0$.

Assumption A2: This condition is apparently satisfied because of (73).

Assumption A3: It has already been proved that the equilibrium point $s = 0$ is GES. This means that if we rewrite the time-derivative of the LFC as

$$\dot{V}_2 \leq -k_d s^2 \quad \forall s \quad (78)$$

then the solutions will satisfy

$$|s(t)| \leq \lambda |s(t_o)| e^{-2(t-t_o)} \quad (79)$$

and therefore by choosing $\nu(|s(t_o)|) = (\lambda/2)|s(t_o)|$ the integrability condition is satisfied.

Since all three assumptions are satisfied and, in addition to this, the nominal system Σ_1 has a globally κ-exponentially stable equilibrium and the system Σ_2 has a GES equilibrium, we conclude from [50, Lemma 8] that the cascade system has a globally κ-exponentially stable equilibrium at $\mathbf{x} = \mathbf{0}$. ■

VII. Compensation of Drift Angle for Heading Control

A. Introduction

The drift, or sideslip, angle β is defined as the angle from the x_b axis of the body-frame o_b to the velocity vector of the vehicle [4, Ch. 2]. In plain words, the drift angle is the angle between the direction toward, which the vehicle is looking (i.e., the orientation described by the heading angle ψ) and the direction toward, which the vehicle is moving (i.e., the orientation described by the course angle χ)

$$\beta = \chi - \psi. \quad (80)$$

This deviation between the heading and the course angle can be attributed to the sway velocity component, which contributes to a variation of the overall velocity vector orientation. In the case where no external forces affect the motion of the vehicle, the sideslip angle occurs due to the lateral acceleration while turning and can be computed, as in (38), repeated here

$$\beta = \mathrm{atan2}(v, u). \quad (81)$$

In the presence of external forces, such as currents with velocity components u_c, v_c for instance, the drift angle will also depend on the relative velocities

$$\beta_c = \mathrm{atan2}(v_r, u_r) \quad (82)$$

where $u_r = u - u_c$ and $v_r = v - v_c$.

In Section IV, it turned out from the stability analysis of the guidance system that, for a vehicle governed by the kinematic equations (15)–(17), the LOS steering law is required to include a term related to the drift angle to stabilize the cross-track error dynamics around the desired equilibrium point (that is, $y_e = 0$). It is therefore important to stress the fact that the drift angle compensation needs to be done whether there are external forces acting on the vehicle or not. The latter case is not always treated in a similar way in the literature because, depending on the position of the origin of the coordinate system considered, it is possible to assume that the effect of the sway velocity due to turning is zero, see for instance [27] and [51]. In these papers, the authors proved κ-exponential stability of the cascade structure consisting of the guidance system and the heading controller. This is a very useful result, especially since it is not always possible to measure or estimate the drift angle. However, considering (81) whenever possible should improve the rate of convergence of the path-following method.

The rest of this section deals with the following two alternatives that make it possible to tackle the drift angle issue and thus compensate for its influence.

1) Direct measurement of β.
2) Integral LOS guidance.

The feasibility and/or effectiveness of each one of the aforementioned techniques largely depends on the available instrumentation, among other things.

B. Direct Measurement of β

The most straightforward and effective way of solving the drift angle problem would be to measure β and use this value in (45). This is the approach we implemented in Section V. In some cases, this could be achieved using optical correlation sensors but these are very expensive, thus making this option difficult to realize. In the absence of environmental forces, the sideslip angle is given by (81) and this means that knowing the values of u, v is sufficient. The simplest way to get these values is to use accelerometers to take measurements of the longitudinal and the lateral acceleration and then calculate the respective velocities by integrating these measurements, see for instance [52] and [53]. The main drawback of this approach, though, is the fact that accelerometer measurements are noisy and also include errors due to the accelerometer bias, hence resulting in large accumulated errors during long-term operations.

A global navigation satellite system (GNSS) can be employed so as to calculate the drift angle more accurately. A GNSS receiver is able to give velocity measurements by either measuring the Doppler shift of the GNSS carrier wave or by measuring the carrier phase difference between the two successive samples [54]. This means that it is not necessary to differentiate the GNSS position measurements. Daily and Bevly [55] show that it is possible to determine experimentally the sideslip angle by taking the difference between the GNSS velocity heading and the vehicle heading calculated by integrating the yaw rate measurements of a gyroscope

$$\beta = \psi_{\text{gyro}} - \psi_{\text{GNSS}}. \tag{83}$$

In this case, the gyro bias should be eliminated while moving along straight segments of the path, otherwise the error due to the integration will accumulate fast. Apart from the simple treatment described by (83), more accurate solutions can be attained by inertial navigation systems sensors aided by GNSS velocity measurements, an implementation of which can be found in [56]. This method uses a state estimator to fuse the several measurements and has the advantage that it does not require a model of the vehicle. It is also worth noting that a GNSS system with two antennas can compute the vehicle heading. This could be an alternative so as to avoid using the gyroscope in (83). Observer-based techniques have been used extensively in the past to address the problem of estimating the drift angle. The interested reader can find more detailed information in [57] and [58].

Despite the variety of the aforementioned options, the problem is far more difficult to tackle when environmental forces act on the vehicle. To illustrate this, imagine a ship that moves forward with zero sway velocity. The existence of a current with $v_c \neq 0$ can introduce a sway velocity component and eventually a drift angle, as it can be concluded by (82). The GNSS approach shown in (83) would not provide the user with sufficient accuracy anymore, because in addition to the ground speed components, the current velocity components should be measured as well. Measuring ocean currents from a moving ship is often a difficult and expensive task. Acoustic Doppler current profilers and electromagnetic current meters are nowadays frequently installed on marine craft to attain estimations of current velocities for a range of depths [59], [60]. It is not difficult to realize that when more factors enter our problem, most commonly wave or wind forces, the level of complexity increases a lot, especially when we are interested in unmanned vehicles applications where space limitations often impose constraints on the allowed onboard equipment.

C. Integral LOS Guidance

An alternative approach that aims at alleviating the sideslip angle effects is the integral LOS guidance [34]. As the name indicates, the conventional LOS guidance is extended by adding integral action, more specifically the integral of the cross-track error y_e or a function of it. Therefore, even when $y_e = 0$ there will be a sideslip angle generation due to the nonzero integral term, which accumulates because of the action of constant disturbances that tend to take the vehicle away from the desired path. The concept of adding integral action to the LOS guidance law is discussed in [1]. Børhaug *et al.* [34] proposed a new integral LOS approach and considered both the kinematic and dynamic aspects of path-following when the task is to converge to a straight-line. By implementing this technique, we avoid the instrumentation requirements presented in Section VII-B. In this section, we will present a modified version of the integral LOS algorithm based on the system kinematics. The following integral LOS

guidance system is proposed:

$$\begin{aligned}\chi &= \gamma_p - \arctan(K_p y_e + K_i y_{\text{int}}) \\ &= \gamma_p - \arctan\left(\frac{1}{\Delta}(y_e + \kappa y_{\text{int}})\right) \end{aligned} \tag{84}$$

$$\dot{y}_{\text{int}} = \frac{U y_e}{\sqrt{\Delta^2 + (y_e + \kappa y_{\text{int}})^2}} \tag{85}$$

where $K_p = (1/\Delta)$, $K_i = K_p \kappa$ and $\kappa > 0$ is a design parameter.

Theorem 2 (Globally κ-Exponentially Stable Integral LOS Guidance Law): The origin $y_e = 0$ of the system (44) is globally κ-exponentially stable under the influence of constant environmental disturbances if the desired course angle is given by (84) and the time-derivative of the integral term is described by (85).

Proof: We can rewrite (44) as follows:

$$\begin{aligned}\dot{y}_e &= U \sin(\psi - \gamma_p + \beta) \\ &= U \sin(\chi - \gamma_p) \\ &= U \sin\left(-\arctan\left(\frac{y_e + \kappa y_{\text{int}}}{\Delta}\right)\right) \end{aligned} \tag{86}$$

and since

$$\sin(\arctan(x)) = x/(\sqrt{x^2+1}) \tag{87}$$

we get

$$\dot{y}_e = -U \frac{y_e + \kappa y_{\text{int}}}{\sqrt{\Delta^2 + (y_e + \kappa y_{\text{int}})^2}}. \tag{88}$$

Next, we propose the LFC

$$V_{\text{int}} = \frac{1}{2} y_e^2 + \frac{1}{2} \kappa y_{\text{int}}^2 \tag{89}$$

and its time-derivative is computed as

$$\begin{aligned}\dot{V}_{\text{int}} &= y_e \left(-U \frac{y_e + \kappa y_{\text{int}}}{\sqrt{\Delta^2 + (y_e + \kappa y_{\text{int}})^2}}\right) + \kappa y_{\text{int}} \dot{y}_{\text{int}} \\ &= -U \frac{y_e^2}{\sqrt{\Delta^2 + (y_e + \kappa y_{\text{int}})^2}} \\ &\quad + \frac{\kappa y_{\text{int}} \left(\dot{y}_{\text{int}} \sqrt{\Delta^2 + (y_e + \kappa y_{\text{int}})^2} - U y_e\right)}{\sqrt{\Delta^2 + (y_e + \kappa y_{\text{int}})^2}}. \end{aligned} \tag{90}$$

Choosing $\dot{y}_{\text{int}}$ as in (85) finally yields

$$\dot{V}_{\text{int}} = -U \frac{y_e^2}{\sqrt{\Delta^2 + (y_e + \kappa y_{\text{int}})^2}} \leq 0. \tag{91}$$

From (91), we can conclude that under the integral LOS guidance law (84) and (85), the system (88) has a UGAS and ULES equilibrium point at $y_e = 0$. ■

In this case, the integral action acts on a kinematic level, since it is part of the LOS guidance. For the use of integral and adaptive actions on a dynamic level and a thorough comparison of several existing methods, the reader is referred to [61].

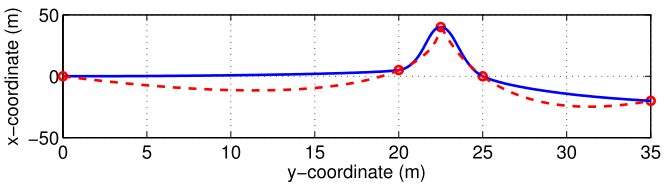

Fig. 5. CHSI method (solid blue line) generates more practical paths compared with a natural cubic spline (dashed red line).

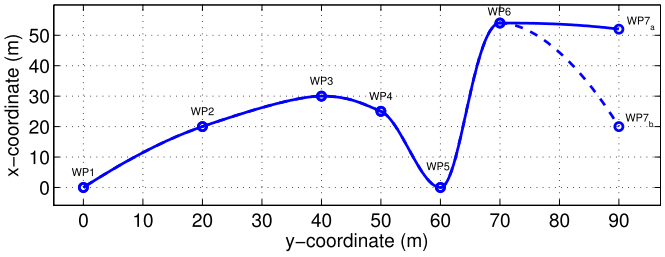

Fig. 6. Local control and monotonicity of the implemented path-planning method are shown. The last waypoint of the initial path has changed, but in a way such that the lines WP6-WP7$_a$ and WP6-WP7$_b$ have slopes of the same sign. This change does not affect the overall shape of the initial path.

VIII. Simulations

The path-planning method, as well as the LOS guidance laws presented in the previous sections, were simulated in MATLAB to test their effectiveness. As mentioned earlier, the CHSI can give more practical paths with a fewer wiggles compared with some curvature-continuous spline methods, a simple example is shown in Fig. 5 where the CHSI is compared with the natural cubic spline. The ability of the implemented cubic Hermite piecewise interpolation to produce monotone paths and provide the user with local control over the path is shown in Fig. 6. The figure depicts two paths, the initial path (WP1-WP7$_a$) and the modified path (WP1-WP7$_b$). The two paths coincide until the 6th waypoint and then split, due to a decision to follow a different route. This could occur at a scenario where a vehicle follows a predefined path navigating between the waypoints 5 and 6 but, during operation, some new data concerning the trajectory between waypoints 6 and 7 (related to weather conditions, or providing information about obstacles) arrive and result in a modification of the desired path. Then the vehicle will not have to change the way it approaches waypoint 6. This would not have been the case with a natural cubic spline, for instance. The local control property does not hold in all cases though. In Fig. 6, the slope of the line connecting WP6-WP7$_b$ has the same sign with the slope of the line connecting WP6-WP7$_a$. In Fig. 7, the lines connecting WP6-WP7$_a$ and WP6-WP7$_c$ have different signs and this causes a variation of only one segment of the whole path (WP5-WP6), hence the partial control term. The new segment, however, is still very close to the initial one and does not require that the vehicle changes its position or orientation very fast. As far as the shape of the path is concerned, the path produced by the Fritsch–Carlson method passes through all the selected waypoints and preserves the monotonicity between each pair of waypoints

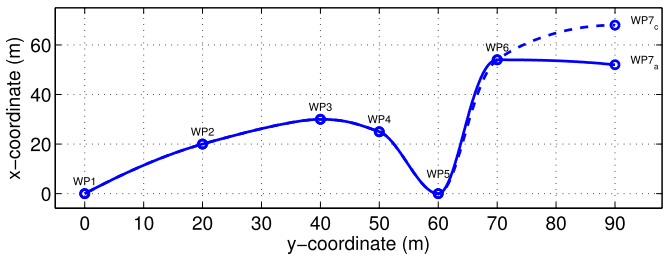

Fig. 7. Partial local control of the monotone CHSI method is shown. In this case, the last waypoint of the initial path changes in a way such that the slopes of WP6-WP7$_a$ and WP6-WP7$_c$ have a different sign. This causes a small change at the segment WP5-WP6.

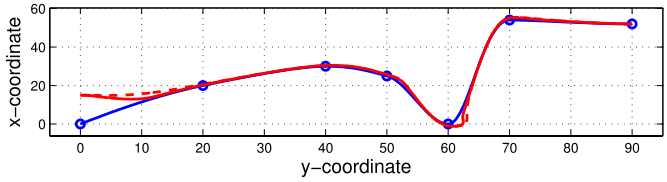

Fig. 8. Path following comparison between the constant Δ (dashed red line) and the variable Δ (solid red line) approach.

without wiggling of zigzagging. This is attributed to the first derivative constraints mentioned in Section II and results in a more practical and tractable path, even though the second derivative continuity is not satisfied.

A nonlinear 3-DOF model has been used for simulating the vehicle's motion. The ability of the proposed variable Δ method to guide the vehicle on the curved path is shown in Fig. 8 and compared with the constant Δ algorithm. In this case, we have omitted the compensation of β since it often might not be available in practice, but this omission downgrades the performance of both guidance methods and therefore the comparison can be considered as a fair one. The parameters were chosen as $\Delta_{\min} = 4$ m, $\Delta_{\max} = 10$ m and $\kappa_\Delta = 1$. For the conventional LOS implementation, we set $\Delta = 7$ m. It can be observed that due to the availability of a range of values for Δ, the variable lookahead method can contribute to meeting the path a bit faster than the constant Δ case. In addition to this, the proposed method results in improved performance when more difficult maneuvering is needed. This is shown more clearly in Fig. 9, which shows a zoomed in portion of the previous picture close to waypoint 5, but this time, for the sake of completeness, the case of a time-varying Δ plus β compensation has also been included.

As it is expected, we observe that the time-varying Δ approach induces a smaller cross-track error than constant $\Delta = 7$ does. It is also natural that the compensation of the sideslip angle (purely due to sway in this case) offers extra information to the control system and improves the performance even further; this can be of critical importance for applications to highly accelerated vehicles.

Fig. 10 shows how the lookahead distance varies during the operation. When the simulation starts, the craft is far from the desired path and, consequently, a low Δ is assigned. As mentioned before, this explains why the craft meets the path faster than it does with a constant Δ. It should also

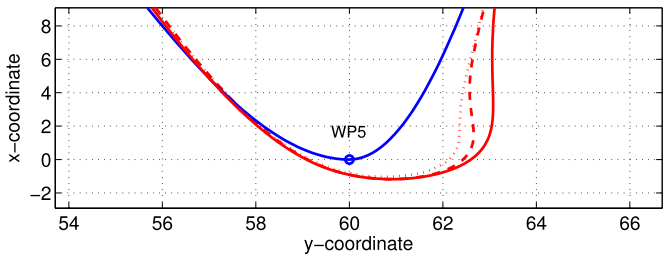

Fig. 9. Performance comparison on a steep turn at waypoint 5 between the constant Δ (solid red line), the variable Δ (dashed red line), and the variable Δ including β (due to turning) compensation (dotted red line) approach.

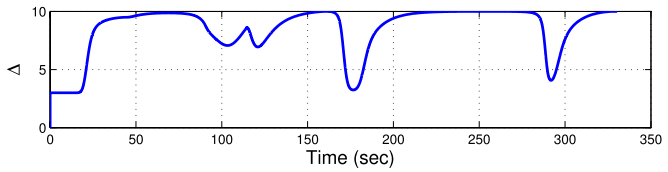

Fig. 10. Time-varying lookahead distance.

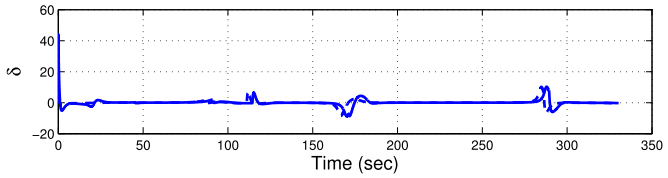

Fig. 11. Comparison of the control variable δ between the variable lookahead distance method (solid blue line) and the conventional algorithm (dashed blue line).

be noted that if a constant low Δ value is assigned, then the vehicle will have an overall aggressive behavior and this will induce an oscillatory behavior around the path. This was demonstrated in [33] where the task for a Mariner class vessel was to converge to a straight line. Moreover, Fig. 10 shows that when the marine craft is close to the path, Δ is close to its maximum value and usually drops at the waypoints. This happens because the second derivative continuities result in step increases of the cross track error and the Δ value decreases to compensate for this.

It should be mentioned that in real life applications, it would be normal to see a sudden drop of Δ from $\Delta_{\max}$ when the craft meets the path, especially during the first approach. The reason for this is that, especially for large and heavy craft, the heading dynamics will take more time to converge, hence the true heading will not be equal to the desired heading when the craft reaches the path. Therefore, the craft will deviate a bit from the path right after reaching it and Δ will react by decreasing right after reaching its maximum value. This behavior was also demonstrated in [33]. Fig. 11 depicts the control signal δ for both cases. It can be concluded that no significant changes occur.

Finally, Fig. 12 shows the effectiveness of the integral LOS guidance law derived in Section VII-C. In this test, the task was chosen to be convergence to a straight line so as to get a better idea about the offset created by the time-invariant external disturbances, as well as the time the integral LOS

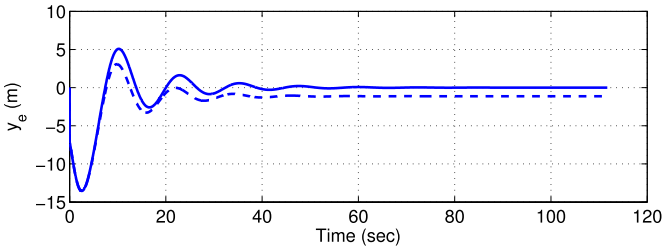

Fig. 12. Cross-track error induced by constant environmental disturbances for conventional LOS guidance (dashed line) and the proposed integral LOS guidance law (solid line).

described by (84) and (85) needs to converge. The external disturbance is considered to be a constant sea current coming from the East and the desired path is a straight line passing through the waypoints $\mathrm{WP}_1(0, 0)$ and $\mathrm{WP}_2(300, 300)$. The initial position and orientation of the marine craft are $P_0(20, 10)$ and $\psi_0 = 0$ rad, respectively. The total speed is $U = 5$ m/s. If no integral action is applied, the induced cross-track error is approximately 1.5 m on the west side of the target line, hence the negative sign. The integral LOS, on the other hand, with $\kappa = 0.1$ manages to eliminate this offset and the vehicle converges to the desired line in approximately 60 s.

IX. Conclusion

This paper has dealt with two interrelated problems pertaining to a vehicle's three DOF planar motion, namely, the path-planning problem, and the LOS guidance problem. Regarding the path-planning issue, we proposed a method to design paths based on the monotone cubic Hermite interpolation method developed by Fritsch and Carlson. As it was shown by simulations, this technique can be very useful for real-time path-planning because gives the freedom to replan segments of the trajectory without requiring the modification of the whole path. Furthermore, it preserves monotonicity between the two successive waypoints, a property that results in segments without unnecessary wiggles and zigzags, as it would be the case if a global control spline interpolation method had been used. On the downside, the proposed method does not satisfy any curvature continuity constraints at the waypoints.

Regarding the LOS guidance problem, we presented a simple extension of the conventional approach by proposing a time-varying lookahead distance Δ, which depends on the cross-track error and a few tuning constants. This contributed to obtaining a more flexible approach, since different lookahead distances result in different maneuvering behaviors. The theoretical analysis showed that, under the assumption of a constant speed U, the overall system consisting of the heading autopilot and the guidance system is forward complete and, as such, its stability properties can be analyzed by using cascaded systems theory. We proved that the overall system has a κ-exponentially stable equilibrium point and, moreover, the stability analysis showed by very simple proofs (based on amplitude-phase form of the cross-track error) how the system has a better inherent stability when the sideslip angle β is compensated for. In a similarly simple way, we were able to derive a new integral LOS guidance law capable of eliminating the cross-track error induced by constant external disturbances.

Future work includes augmenting the methods discussed here so as to be able to address path-tracking tasks where time constraints enter the problem as well, and the speed control system has to be considered. Moreover, it would be useful to develop a method that will help the user decide upon how to choose the values of the tuning parameters. It is also possible to test different functions for Δ and compare their performances. Regarding the path-planning part, a natural continuation is to extend the presented paths to 3-D space. In that case it would be of interest to investigate whether the monotonicity property and the practicality of the paths based on the Fritsch and Carlson method still hold.

Appendix
Cascaded Systems Theory

In this section, we present the theorem, which was employed in Section VI-B to show stability of the cascade. The proof can be found in [47] and in our case we include a reformulated version, like the one which was used in [49].

Consider the cascade system

$$\Sigma_1 : \dot{x}_1 = f(t, x_1) + g(t, x)x_2 \tag{92}$$

$$\Sigma_2 : \dot{x}_2 = f(t, x_2) \tag{93}$$

where $x_1 \in R^n, x_2 \in R^m, x \triangleq [x_1, x_2]^T$. The function $f(t, x_1)$ is continuously differentiable in (t, x_1) and $f(t, x_2), g(t, x)$ are continuous in their arguments and locally Lipschitz.

Theorem A: The cascaded system (92) and (93) is globally uniformly asymptotically stable if the following three assumptions are satisfied.

A1) The system $f(t, x_1)$ is globally uniformly asymptotically stable with a Lyapunov function $V(t, x_1)$, $V : R_{\geq 0} \times R^n \rightarrow: R_{\geq 0}$ positive definite (that is $V(t, 0) = 0$ and $V(t, x_1) > 0 \quad \forall x_1 \neq 0$) and proper (that is, radially unbounded), which satisfies

$$\left\| \frac{\partial V}{\partial x_1} \right\| \|x_1\| \leq c_1 V(t, x_1) \quad \forall \|x_1\| \geq \mu \quad \text{where } c_1, \mu > 0. \tag{94}$$

We also assume that $(\partial V/\partial x_1)(t, x_1)$ is bounded uniformly in t for all $\|x_1\| \leq \mu$, that is, there exists a constant $c_2 > 0$ such that for all $t \geq t_o \geq 0$

$$\left\| \frac{\partial V}{\partial x_1} \right\| \leq c_2 \quad \forall \|x_1\| \leq \mu. \tag{95}$$

A2) The function $g(t, x)$ satisfies

$$\|g(t, x)\| \leq \theta_1(\|x_2\|) + \theta_2(\|x_2\|)\|x_1\| \tag{96}$$

where $\theta_1, \theta_2 : R_{\geq 0} \rightarrow R_{\geq 0}$ are continuous.

A3) Equation $\dot{x}_2 = f(t, x_2)$ is globally uniformly asymptotically stable and for all $t_o \geq 0$

$$\int_{t_o}^{\infty} \|x_2(t, t_o, x_2(t_o))\| \, dt \leq \phi(\|x_2(t_o)\|). \tag{97}$$

It was shown in [50] that, if in addition to the assumptions in Theorem A, both $\dot{x}_1 = f(t, x_1)$ and $\dot{x}_2 = f(t, x_2)$ are globally κ-exponentially stable, then the cascaded system (92) and (93) is globally κ-exponentially stable.

REFERENCES

[1] M. Breivik and T. I. Fossen, *Guidance Laws for Autonomous Underwater Vehicles*. Underwater Vehicles, A. V. Inzartsev, Ed. Vellore, India: INTECH Education Publishing, 2009, pp. 51–76, ch. 4.

[2] R. Yanushevsky, *Guidance of Unmanned Aerial Vehicles*. Cleveland, OH, USA: CRC Press, 2011.

[3] M. Breivik, "Topics in guided motion control of marine vehicles," Ph.D. dissertation, Dept. Eng. Cybern., Norwegian Univ. Sci. Technol., Trondheim, Norway, 2010.

[4] T. I. Fossen, *Handbook of Marine Craft Hydrodynamics and Motion Control*. New York, NY, USA: Wiley, 2011.

[5] L. E. Dubins, "On curves of minimal length with a constraint on average curvature, and with prescribed initial and terminal positions and tangents," *Amer. J. Math.*, vol. 79, no. 3, pp. 497–516, 1957.

[6] J. A. Reeds and L. A. Shepp, "Optimal paths for a car that goes both forwards and backwards," *Pacific J. Math.*, vol. 145, no. 2, pp. 367–393, 1990.

[7] L. Techy and C. A. Woolsey, "Minimum-time path planning for unmanned aerial vehicles in steady uniform winds," *J. Guid., Control, Dyn.*, vol. 32, no. 6, pp. 1736–1746, 2009.

[8] G. Ambrosino, M. Ariola, U. Ciniglio, F. Corraro, E. De Lellis, and A. Pironti, "Path generation and tracking in 3-D for UAVs," *IEEE Trans. Control Syst. Technol.*, vol. 17, no. 4, pp. 980–988, Jul. 2009.

[9] J. D. Boissonnat, A. Cerezo, and J. Leblond, "A note on shortest paths in the plane subject to a constraint on the derivative of the curvature," INRIA, Paris, France, Tech. Rep. 2160, 1994.

[10] T. Fraichard and A. Scheuer, "From Reeds and Shepp's to continuous-curvature paths," *IEEE Trans. Robot.*, vol. 20, no. 6, pp. 1025–1035, Dec. 2004.

[11] R. T. Farouki and T. Sakkalis, "Pythagorean hodographs," *IBM J. Res. Develop.*, vol. 34, no. 5, pp. 736–752, Sep. 1990.

[12] H. Bruyninckx and D. Reynaerts, "Path planning for mobile and hyper-redundant robots using pythagorean hodograph curves," in *Proc. 8th Int. Conf. Adv. Robot.*, 1997, pp. 595–600.

[13] A. Tsourdos, B. White, and M. Shanmugavel, *Cooperative Path Planning of Unmanned Aerial Vehicles*. New York, NY, USA: Wiley, 2011.

[14] A. Dahl, "Path planning and guidance for marine surface vessels," M.Sc. thesis, Inst. Teknisk Kybernetikk, Norwegian Univ. Sci. Technol., 2013.

[15] A. M. Lekkas, A. R. Dahl, M. Breivik, and T. I. Fossen, "Continuous-curvature path generation using Fermat's spiral," *Model., Identificat. Control*, vol. 34, no. 4, pp. 183–198, 2013.

[16] K. G. Jolly, R. S. Kumar, and R. Vijayakumar, "A Bezier curve based path planning in a multi-agent robot soccer system without violating the acceleration limits," *Robot. Auto. Syst.*, vol. 57, no. 1, pp. 23–33, 2009.

[17] C. L. Bottasso, D. Leonello, and B. Savini, "Path planning for autonomous vehicles by trajectory smoothing using motion primitives," *IEEE Trans. Control Syst. Technol.*, vol. 16, no. 6, pp. 1152–1168, Nov. 2008.

[18] E. P. Anderson, R. W. Beard, and T. W. McLain, "Real-time dynamic trajectory smoothing for unmanned air vehicles," *IEEE Trans. Control Syst. Technol.*, vol. 13, no. 3, pp. 471–477, May 2005.

[19] E. Frazzoli, M. A. Dahleh, and E. Feron, "Real-time motion planning for agile autonomous vehicles," *J. Guid., Control, Dyn.*, vol. 25, no. 1, pp. 116–129, 2002.

[20] M. Mattei and L. Blasi, "Smooth flight trajectory planning in the presence of no-fly zones and obstacles," *J. Guid., Control, Dyn.*, vol. 33, no. 2, pp. 454–462, 2010.

[21] M. Candeloro, A. M. Lekkas, A. J. Sørensen, and T. I. Fossen, "Continuous curvature path planning using Voronoi diagrams and Fermat's spirals," in *Proc. 9th IFAC Conf. Control Appl. Marine Syst.*, Osaka, Japan, 2013, pp. 132–137.

[22] T. I. Fossen, M. Breivik, and R. Skjetne, "Line-of-sight path following of underactuated marine craft," in *Proc. 6th IFAC Conf. Manoevring Control Marine Craft*, Girona, Spain, 2003, pp. 244–249.

[23] C.-K. Ryoo, H. Cho, and M.-J. Tahk, "Optimal guidance laws with terminal impact angle constraint," *J. Guid., Control, Dyn.*, vol. 28, no. 4, pp. 724–732, 2005.

[24] C.-K. Ryoo, H.-S. Shin, and M.-J. Tahk, "Energy optimal waypoint guidance synthesis for antiship missiles," *IEEE Trans. Aerosp. Electron. Syst.*, vol. 46, no. 1, pp. 80–95, Jan. 2010.

[25] A. J. Healey and D. Lienard, "Multivariable sliding mode control for autonomous diving and steering of unmanned underwater vehicles," *IEEE J. Ocean. Eng.*, vol. 18, no. 3, pp. 327–339, Jul. 1993.

[26] M. Breivik and T. I. Fossen, "Path following for marine surface vessels," in *Proc. IEEE Technol. Ocean.*, Kobe, Japan, Nov. 2004, pp. 2282–2289.

[27] E. Børhaug and K. Y. Pettersen, "Cross-track control for underactuated autonomous vehicles," in *Proc. 44th IEEE Conf. Decision Control, Eur. Control Conf.*, Seville, Spain, Dec. 2005, pp. 602–608.

[28] O. J. Sørdalen and O. Egeland, "Exponential stabilization of nonholonomic chained systems," *IEEE Trans. Autom. Control*, vol. 40, no. 1, pp. 35–49, Jan. 1995.

[29] E. Børhaug, A. Pavlov, E. Panteley, and K. Y. Pettersen, "Straight line path following for formations of underactuated marine surface vessels," *IEEE Trans. Control Syst. Technol.*, vol. 19, no. 3, pp. 493–506, May 2011.

[30] M. Breivik and T. I. Fossen, "Principles of guidance-based path following in 2D and 3D," in *Proc. 44th IEEE Conf. Decision Control, Eur. Control Conf.*, Seville, Spain, Dec. 2005, pp. 627–634.

[31] A. Pavlov, H. Nordahl, and M. Breivik, "MPC-based optimal path following for underactuated vessels," in *Proc. 8th IFAC Int. Conf. Manoeuvring Control Marine Craft*, Guaruja, Brazil, 2009, pp. 340–345.

[32] S. R. Oh and J. Sun, "Path following of underactuated marine surface vessels using line-of-sight based model predictive control," *Ocean Eng.*, vol. 37, nos. 2–3, pp. 289–295, 2010.

[33] A. M. Lekkas and T. I. Fossen, "A time-varying lookahead distance guidance law for path following," in *Proc. 9th IFAC Conf. Manoeuvring Control Marine Craft*, Arenzano, Italy, 2012, pp. 398–403.

[34] E. Børhaug, A. Pavlov, and K. Y. Pettersen, "Integral LOS control for path following of underactuated marine surface vessels in the presence of constant ocean currents," in *Proc. 47th IEEE Conf. Decision Control*, Cancun, Mexico, Dec. 2008, pp. 4984–4991.

[35] F. N. Fritsch and R. E. Carlson, "Monotone piecewise cubic interpolation," *SIAM J. Numer. Anal.*, vol. 17, no. 2, pp. 238–246, 1980.

[36] F. A. Papoulias, "Bifurcation analysis of line of sight vehicle guidance using sliding modes," *Int. J. Bifurcation Chaos*, vol. 1, no. 4, pp. 849–865, 1991.

[37] C. B. Moler, *Numerical Computing with MATLAB*. Philadelphia, PA, USA: Soc. Ind. Math., 2004.

[38] D. Walton and D. Meek, "Curvature extrema of planar parametric polynomial cubic curves," *J. Comput. Appl. Math.*, vol. 134, no. 1, pp. 69–83, 2001.

[39] K. Yang and S. Sukkarieh, "An analytical continuous-curvature path-smoothing algorithm," *IEEE Trans. Robot.*, vol. 26, no. 3, pp. 561–568, Jun. 2010.

[40] M. Breivik, V. E. Hovstein, and T. I. Fossen, "Straight-line target tracking for unmanned surface vehicles," *Model., Identificat. Control*, vol. 29, no. 4, pp. 131–149, 2008.

[41] L. Lapierre, D. Soetanto, and A. Pascoal, "Nonlinear path following with applications to the control of autonomous underwater vehicles," in *Proc. 42nd IEEE Conf. Decision Control*, Maui, HI, USA, Dec. 2003, pp. 1256–1261.

[42] D. Soetanto, L. Lapierre, and A. Pascoal, "Adaptive, non-singular path-following control of dynamic wheeled robots," in *Proc. 42nd IEEE Conf. Decision Control*, Maui, HI, USA, Dec. 2003, pp. 1765–1770.

[43] E. Lefeber, "Tracking control of nonlinear mechanical systems," Ph.D. dissertation, Faculty Math. Sci., Univ. Twente, Enschede, Netherlands, 2000.

[44] N. Norrbin, "On the design and analysis of the zig-zag test on base of quasi-linear frequency response," The Swedish State Shipbuilding Experimental Tank, Gothenburg, Sweden, Tech. Rep. B 104-3, 1963.

[45] V. Utkin, "Variable structure systems with sliding modes," *IEEE Trans. Autom. Control*, vol. 22, no. 2, pp. 212–222, Apr. 1977.

[46] R. A. DeCarlo, S. H. Zak, and G. P. Matthews, "Variable structure control of nonlinear multivariable systems: A tutorial," *Proc. IEEE*, vol. 76, no. 3, pp. 212–232, Mar. 1988.

[47] E. Panteley and A. Loría, "On global uniform asymptotic stability of nonlinear time-varying systems in cascade," *Syst., Control Lett.*, vol. 33, no. 2, pp. 131–138, 1998.

[48] D. Angeli and E. D. Sontag, "Forward completeness, unboundedness observability, and their Lyapunov characterizations," *Syst., Control Lett.*, vol. 38, no. 4, pp. 209–217, 1999.

[49] A. Loría, T. I. Fossen, and E. Panteley, "A separation principle for dynamic positioning of ships: Theoretical and experimental results," *IEEE Trans. Control Syst. Technol.*, vol. 8, no. 2, pp. 332–343, Mar. 2000.

[50] E. Panteley, E. Lefeber, A. Loría, and H. Nijmeijer, "Exponential tracking control of a mobile car using a cascaded approach," in *Proc. IFAC Workshop Motion Control*, 1998, pp. 221–226.

[51] E. Fredriksen and K. Y. Pettersen, "Global κ-exponential way-point maneuvering of ships: Theory and experiments," *Automatica*, vol. 42, no. 4, pp. 677–687, 2006.

[52] V. Alberti and E. Babbel, "Improved driving stability by active braking of the individual wheels," in *Proc. Int. Symp. Adv. Veh. Control*, 1996, pp. 717–732.

[53] A. Hac and M. D. Simpson, "Estimation of vehicle side slip angle and yaw rate," in *Proc. SAE World Congr.*, 2000, pp. 1032–1038.

[54] E. D. Kaplan and C. J. Hegarty, *Understanding GPS: Principles and Applications*. Norwood, MA, USA: Artech House Publishers, 2006.

[55] R. Daily and D. M. Bevly, "The use of GPS for vehicle stability control systems," *IEEE Trans. Ind. Electron.*, vol. 51, no. 2, pp. 270–277, Apr. 2004.

[56] D. M. Bevly, R. Sheridan, and J. C. Gerdes, "Integrating INS sensors with GPS velocity measurements for continuous estimation of vehicle sideslip and tire cornering stiffness," in *Proc. Amer. Control Conf.*, 2001, pp. 25–30.

[57] J. Stephant, A. Charara, and D. Meizel, "Virtual sensor: Application to vehicle sideslip angle and transversal forces," *IEEE Trans. Ind. Electron.*, vol. 51, no. 2, pp. 278–289, Apr. 2004.

[58] H. F. Grip, L. Imsland, T. A. Johansen, J. C. Kalkkuhl, and A. Suissa, "Vehicle sideslip estimation," *IEEE Control Syst. Mag.*, vol. 29, no. 5, pp. 36–52, Oct. 2009.

[59] J. Candela, R. C. Beardsley, and R. Limeburner, "Separation of tidal and subtidal currents in ship-mounted acoustic Doppler current profiler observations," *J. Geophys. Res.*, vol. 97, no. C1, pp. 769–788, 1992.

[60] J. M. Fulford, K. G. Thibodeaux, and W. R. Kaehrle, "Comparison of current meters used for stream gaging," in *Proc. ASCE Symp.*, Buffalo, NY, USA, 1994, pp. 376–385.

[61] G. Antonelli, "On the use of adaptive/integral actions for six-degrees-of-freedom control of autonomous underwater vehicles," *IEEE J. Ocean. Eng.*, vol. 32, no. 2, pp. 300–312, Apr. 2007.